The Optical Design for Cryoscope: a wide-field NIR telescope with low thermal emission

Jason Fucik and Roger Smith

Caltech Optical Observatories, 1200 E. California Blvd., Pasadena, CA 91125

ABSTRACT

We present the optical design for Cryoscope, a 0.26 m aperture telescope that is a f/2 objective operating over the photometric K band (1.99 to 2.55 μ m) with diffraction limited imaging. It has a 16 deg² FoV with a 7.1"/pix plate scale on a 2048×2048 18 μ m/pixel Teledyne H2RG detector array. The objective is a catadioptric design incorporating two thin fused silica meniscus lenses near the entrance aperture, a spherical primary mirror, and a doublet immediately in front of the detector to flatten the image surface. The design solution is capable of delivering diffraction limited images over a 10° field diameter at f/1.25 in the NIR. The use of fused silica for the first two lens elements allows the design to be used for a broad range of applications from the vacuum ultraviolet to thermal IR with only re-optimization of the field flattening doublet. In the VUV (185 to 300 nm) the design is no longer diffraction limited, but can still be made to be pixel limited with detector arrays having pixels as small as 10 μ m. The design provides a compact, wide field, and fast objective that can scale to a 1 m-class telescope and offers several benefits over a classical Schmidt telescope. The convex fused silica meniscus lens is strong enough to serve as a vacuum window allowing the entire optical path to be cryogenically cooled to maintain low thermal emission while delivering two orders of magnitude larger field of view than previous ground-based designs for the thermal infrared.

Keywords: wide-field, imager, survey telescope, near-infrared, thermal infrared

1. INTRODUCTION

1.1 Overview

This paper introduces a wide field telescope design that uses only fused silica corrector elements to deliver excellent image quality over $50 \, \text{deg}^2$ field of view (FoV) at focal ratio as fast as f/1.2. §1.2 describes the design's original purpose to eliminate CaF_2 from a design optimized for the vacuum ultraviolet in space. §1.3 describes the design's adaption to the NIR where it provides unprecedented FoV for an imaging system with low thermal background. §2 covers the optical design for the Cryoscope implementation in detail, while §3 describes the current status of the larger Cryoscope project. §4 closes with a vision for a facility at Dome C to enable time domain astronomy in the NIR.

1.2 Space-based UV Wide-Field Imager

Initial investigations sought an optical design for a fast (\sim f/1.2) wide field (\ge 10°) telescope that operated in the Vacuum Ultra-Violet (VUV) which could avoid the use of a large Calcium Fluoride (CaF₂) corrector element required by the classical Schmidt objective, which locates two nearly flat aspheric achromatic corrector plates near the aperture stop positioned at the radius of curvature of the primary mirror. The two corrector plates differ in their indices of refraction to control the sphero-chromatism. In the VUV, the only material options for a 0.26 m aperture telescope are CaF₂ and Fused Silica (SiO₂). The design focused on solutions that utilize only SiO₂ corrector elements to avoid the use of CaF₂ which is a dense, thermally sensitive and brittle crystalline material, which becomes very heavy when made thick enough to survive forces experienced during space launch.

The study started by optimizing a f/1.2 (315 mm focal length) Maksutov objective¹ with a single SiO₂ meniscus corrector. The Maksutov design variants suffered from sphero-chromatism and off-axis aberrations that resulted in 80% Encircled Energy (EE) diameter greater than the desired $< 20 \mu m$ (13") at the focal plane

Send correspondence to: jrf@astro.caltech.edu

over the 10° diameter FoV. The Maksutov objective was limited by the axial color, so the study evolved to look at a Baker-Nunn² and Houghton³ objectives. The Houghton objective uses an all spherical doublet or triplet located at the aperture stop. It should be noted that both the Maksutov and Houghton designs were developed as inexpensive alternatives to fabricating the aspheric corrector plate of a Schmidt telescope. The Baker-Nunn objective builds upon the work by Houghton by incorporating aspheric surfaces on the refractive elements (triplet) to get better off-axis field correction of aberrations than what a classical Schmidt objective can deliver (particularly at fast focal ratios $\sim f/1$).

A Baker-Nunn objective uses a pairing of crown and flint glass types for longitudinal color correction. The crown glass is the central negative lens where the flint glass used for the outlying positive lens elements are symmetrically positioned around the center crown glass. The triplet refractive corrector is place symmetrically about the aperture stop of the lens system. The aspheric surfaces for the two positive lenses are placed on the inner convex faces and on both concave faces of the negative lens. The air spacing between the lens elements can be increased to reduce the aspheric deviation (or power) of the surfaces, but comes at the expense of increasing the residual astigmatism. A conventional Baker-Nunn optical prescription could not be used in the study since only designs with SiO₂ corrector elements were being allowed, so this study explored design solutions that remove the negative (central) low dispersion element and maintain the symmetry about the aperture stop. A family of solutions has emerged where the two SiO₂ corrector elements become meniscus shaped with the convex faces pointed towards the aperture stop. By minimizing the air gap between the two corrector elements the new design solution is able to achieve smaller spot sizes for the same focal ratio and field radius than an equivalent Schmidt design. The new design results in a telescope that is $\sim 30\%$ shorter in its overall length. This reduces the diameter of the spherical primary mirror required to prevent vignetting at the edges of the field of view. The meniscus lenses are mechanically stiff even when made relatively thin so that total mass is reduced by about a factor of three when compared to the Schmidt design. For the mass-limited application in space, this enabled the telescope aperture to be increased.

1.3 Ground-based Thermal IR Wide-Field Imager

At room temperature, substantial black-body radiation is emitted by the telescope itself longward of $\sim 2~\mu m$. At locations where the emission from the sky and atmosphere are low it is imperative to also reduce emission by the telescope to maximize sensitivity. This can be achieved by making the telescope very cold, or (as is common for ground based astronomy) by intercepting the thermal emission by attaching a cryogenically cooled re-imaging system to the warm telescope to form an image of the telescope's pupil on a cold mask (Lyot stop) before reforming the object image on the cryogenically cooled infrared sensor. Re-imaging systems typically have a field of view no greater than $\sim 0.05~{\rm deg^2}$. ESO's VISTA telescope does substantially better using a dedicated telescope design with carefully placed reflective baffles, and a long cold snout in front of the focal plane but still only achieves $0.6~{\rm deg^2}$ FoV. To avoid these problems, much of infrared astronomy is done in space, where telescopes can be radiatively cooled to low temperatures, but at great expense. NASA's next flagship telescope, Roman Space Telescope, is described as "wide field" but with only $0.28~{\rm deg^2}$ FoV, it is unsuitable for time domain astronomy, where $> 10~{\rm deg^2}$ instantaneous FoV is required to achieve adequate sky coverage at the required codence of hours to days.

Our design makes cryogenic cooling of the entire optical path possible in terrestrial applications. In addition to diffraction limited imaging over a wide field at a fast focal ratio, the key feature is the existence of a *convex* (or positive) meniscus lens at the entrance which can be used as a vacuum window without becoming unacceptably thick and heavy. When this convex meniscus lens is supported by radial forces applied along a plane perpendicular to the radius of curvature, almost the entire lens is placed in compression, with only minor exceptions where the elastomeric support exerts (acceptably low) shear stress. Fused silica is very strong in compression providing a large factor of safety (>35 for current design) so the meniscus lens can be made as thin as the manufacturing process allows. The size of fused silica blanks is not a limitation, and development underway to slump fused silica of this size holds promise that manufacturing costs will be acceptable at sizes exceeding 1 m.

The cryogenic telescope's thermal emission is limited to that of the transmissive corrector elements near ambient temperature (about -40°C) and that of a low emissivity reflective pupil stop configured so that the focal plane sees its own reflection. The design is being developed for deployment at Dome C, 15° latitude from the

South Pole, where the sky background is approximately $40\times$ darker than at mid-latitudes since the equivalent sky temperature is low enough to shift the onset of black-body emission by the sky to wavelengths beyond 2.55 μ m where water absorption cuts off transmission again. The short edge of the K_{dark} passband is at 2.35 μ m where OH emission drops away.

Our ultimate goal is to deploy a version of this design with ~ 1.1 m aperture (or larger if slumping makes this affordable) on a tower at Dome C where median seeing is 0.25'' allowing the telescope to be diffraction limited, for maximum sensitivity (albeit under-sampled) enabling time domain astronomy at $2.4 \mu m$ (e.g. localize neutron star - black hole mergers which are thought to produce the heavy elements). The feasibility of this project is enhanced by recent developments in infrared detector manufacturing which promise to reduce cost per pixel by as much as a factor of four making feasible the gigapixel focal plane required to populate the 50 deg² field of view at 1''/pixel image scale.

The Cryoscope project is a 0.26 m aperture technology demonstrator that will validate the new optical design, and the low thermal background in K_{dark} band over a wide field size of 16.7 deg². The Cryoscope telescope will first be deployed to Palomar Observatory borrowing the mount for the Gattini-IR⁵ J-band survey, and with further funding will be deployed in the Antractic. Even the technology demonstrator will increase the largest available field of view for a low thermal background NIR imager (0.6 deg² for VISTA IR Camera⁶) by a factor of 27.

2. OPTICAL DESIGN

The original design study was focused on a VUV space-based application, but the design form was re-optimized for the Cryoscope ground-based NIR application. Further refinement of the meniscus corrector elements was done for NIR applications where the objective achieves diffraction-limited image quality (>90% Strehl ratio) at f/1.25 over a 10° field diameter. The Cryoscope project made the design decision for a finer plate scale (7.1"/pix) by increasing the focal length to 525 mm, while keeping the aperture stop sized to 26 cm because of cost constraints. This gave a f/2 telescope design with a >99% Strehl ratio in K-band over the $4^{\circ}\times4^{\circ}$ FoV subtended by the 2048×2048 Teledyne H2RG (18 μ m pixel) NIR sensor available to the project.

2.1 Symmetrical Meniscus Corrector Elements

The meniscus corrector elements are quasi-symmetrical about the aperture stop. Without an achromatic lens pairing, early studies were focused on whether the axial and lateral color aberrations could be sufficiently controlled by a duo of SiO_2 lenses. The best results were found when $R_1 = -R_3$ and $R_2 = -R_4$ for the meniscus pairing as shown in Fig. 1 where the central thickness of each lens were held equal. This symmetry condition does not have to be strictly adhered too and many design variants had asymmetric arrangements, but the symmetric pairing does minimize the curvature on any one meniscus lens which is beneficial for manufacturing purposes. The axial color caused by the first meniscus lens is cancelled by the second meniscus lens. The axial color is well corrected over a broad spectral range (> 1 octave). The limiting chromatic aberration is the lateral color. The lateral color caused by the first surface is canceled by the second surface within each meniscus lens and the lateral color is well corrected within ~ 0.25 octave wide spectral range, which covers imaging within any single photometric passband.

The convex faces on the meniscus lenses are 6th order aspheric surfaces where the sagitta of the surface is described by:

$$z(r) = \frac{r^2/R}{1 + \sqrt{1 - (r/R)^2}} + \alpha_2 r^4 + \alpha_3 r^6 \tag{1}$$

R is the base radius of the surface, α_2 and α_3 are the aspheric coefficients. The aspheric deviation (see Fig.4) from the nearest spherical surface on the meniscus lenses was found to be 3-4× less than Schmidt corrector plates for systems with comparable specifications. The meniscus lens pair with opposing aspheric surfaces corrects for spherical aberration from the primary mirror, as is the case for the classical Schmidt arrangement, without degradation in coma errors.

Table 1: CryoScope Telescope Properties.

Description	Value	
Aperture Stop	260 mm	
Focal Length	525 mm	
Focal Ratio	2.0	
FOV	$4^{\circ} \times 4^{\circ} (16 \text{ deg}^2)$	
Wavelength Range	$1.99 - 2.55 \mu m \text{ (K-band)}$	
Plate Scale	7.1"/pix	
PSF FWHM	$4.8 \ \mu m \ (1.9'')$	
Detector Array	$2048 \times 2048 \text{ pix}^2$	
Pixel Width	$18~\mu\mathrm{m}$	
Median Seeing (Palomar)	1"	
Median Seeing (South Pole)	2"	
Sky Flux/Pixel (Palomar)	14,223 e-/s	
Sky Flux/Pixel (South Pole)	341 e-/s	
Limiting Magnitude (Palomar) SNR=7 in 1000s	17.2	
Limiting Magnitude (South Pole) 19.1		
AB Depth (Palomar) in 60s	15.5	
AB Depth (South Pole)	17.5	
Volumetric Survey Speed (Palomar)	$12 \; {\rm Mpc^3 s^{-1}}$	
Volumetric Survey Speed (South Pole)	$185 \; {\rm Mpc^3 s^{-1}}$	

2.2 Optical Prescription

The catadioptic objective has meniscus lenses with radii of curvature $R_1 = -600$ mm and $R_2 = -670.5$ mm with a center thickness of 12.5 mm (see Table 2). For the 300 mm diameter lenses this gave an aspect ratio of 24:1 between the center thickness and diameter. Discussions with opticians placed this near state-of-the-art with presently available manufacturing facilities. The vertex of the convex face for each meniscus lens is spaced 2.5 mm from the center of the aperture stop. Objects positioned at infinity are then focused by the spherical primary mirror. The spherical mirror has a concave radius of 1124.5 mm with a clear aperture of 341 mm (f/1.65). Most of the optical power in the system is carried by the primary.

A vacuum-spaced achromatic doublet is used to flatten the focal surface of the spherical primary onto a detector array. For K-band imaging, a Zinc Sulfide (ZnS) and SiO_2 lens pair worked well to minimize the field curvature without introducing additional transverse or longitudinal aberrations. Having a SiO_2 lens prior to the detector plane was a design constraint to prevent radioactive emission from reaching the detector that has been measured in other optical glasses.⁷ The field flatter lenses are also meniscus in shape with a 6th order aspheric surface on the convex face. The aspheric surfaces on the field lenses may not be necessary in some applications, but do help to better correct for transverse aberrations. The telescope has a 90 mm diameter central obstruction located behind the detector, which decreases the effective entrance aperture area by $\sim 12\%$.

The optical prescription gives nearly uniform polychromatic diffraction limited image quality in K-band over the $4^{\circ} \times 4^{\circ}$ FoV with a Strehl ratio >99% (see Fig.5). The choice was made to optimize the image quality for the entire K-band to allow the demonstrator to be equipped for either full K-band imaging (simplifying the comparison with existing K-band imagers) or for operation in the narrower K_{dark} passband which is optimal in the Antarctic. The filter coating for one or other of these passbands will be deposited on the concave face of

the second field flattener element which is chosen to distribute the detector-filter ghost over the largest possible area.

The telescope design also has characteristically low distortion. The maximum distortion at the corners of the detector array is <0.02%, which is a maximum displacement of 1.4''(or ~ 0.2 pix) from a rectilinear grid.

Lens	Glass		Radii	Thickness
	n_d	$ u_d$		
I	1.4586	67.6648	$R_1 = -600.0$	$t_1 = 12.5$
			$R_2 = -670.5$	$S_1 = 2.5$
STOP				$S_2 = 2.5$
II	1.4586	67.6648	$R_3 = 600.0$	$t_2 = 12.5$
			$R_4 = 670.5$	$S_3 = 670.0$
M			$R_5 = -1124.5$	$S_4 = -537.0$
III	2.3672	15.3046	$R_6 = -237.3$	$t_3 = -10.0$
			$R_7 = -595.0$	$S_5 = -6.5$
IV	1.4586	67.6648	$R_8 = 241.7$	$t_4 = -10.0$
			$R_9 = 187.7$	$S_6 = BFD$

Table 2: CryoScope Telescope Prescription.

- a) Lens units are in millimeters.
- b) t_i is the axial thickness of the element. S_i is the axial air-spacing.
- c) R_2 , R_3 , R_6 , and R_9 are aspheric surfaces. All other surfaces are spherical.
- d) R_2 aspheric coefficients: $\alpha_2 = 1.6252 \times 10^{-10}$, $\alpha_3 = -1.1097 \times 10^{-15}$
- e) R_3 aspheric coefficients: $\alpha_2 =$ -2.5529×10 $^{-10}$, $\alpha_3 =$ -1.7503×10 $^{-15}$
- f) R_6 aspheric coefficients: $\alpha_2 = -2.9232 \times 10^{-8}$, $\alpha_3 = -1.1975 \times 10^{-12}$
- g) R_9 aspheric coefficients: $\alpha_2 = -1.2044 \times 10^{-7}$, $\alpha_3 = 1.7366 \times 10^{-11}$

3. CRYOSCOPE PROJECT

The 0.26 m aperture demonstrator serves as a quarter to fifth scale prototype of a proposed 1 to 1.2 m-class cryogenic telescope. The demonstrator will verify the delivered imaged quality, limiting stellar magnitude, thermal background suppression, prevention of condensation on the window, and good control of systematic errors like image tilt, focus and flexure. Successful demonstration of these capabilities will open a pathway to a large new parameter space, by allowing the exploration for the first time of the *dynamic* infrared sky. The demonstrator with a modest 26 cm aperture will also be capable of unveiling a wide variety of Galactic science. For every magnitude of extinction in the V-band there is only 0.1 mag of extinction in the K_{dark} passband. This simple fact opens up key science in the Milky Way.

The Cryoscope project has completed a detail design of the detector mount, electronics and opto-mechanical system including a study for the telescope baffling scheme to minimize the thermal background and stray light that reaches the detector (see §3.1). The project is currently in a manufacturing phase (see §3.2) and later this year moving into assembly and test of the optical elements (see §3.3). Completion of the telescope is estimate to be in 2023 with on-sky demonstration at Palomar Observatory.

3.1 Baffling and Stray Light

The second meniscus lens has an ideal shape for supporting large forces (i.e. an arch) caused by atmospheric pressure, and thus can be used as the window to an evacuated telescope tube. This makes practical a radically different approach to suppressing thermal background. The conventional method to prevent thermal radiation emitted by the telescope from reaching the detector is to re-image the telescope pupil onto a cold Lyot stop but

this still suffers from emission by several warm mirrors which have 1-2% emissivity (depending on coating and cleanliness), the telescope spiders and the dewar window. The more serious problem is that the re-imaging optics grow unreasonably large when coupled to a wide field telescope. So, to increase the field of view, ESO's VISTA telescope adopted a long cold baffle and narcissus mirrors to block emission from the warm telescope.⁶ Although this increases the FoV an order of magnitude relative to re-imaging onto a cold Lyot stop, this approach still only achieved 0.6 deg² area on-sky, two orders of magnitude less than required by our science. At the same time this approach does not suppress thermal background from warm mirror surfaces and spiders supporting the secondary mirror.

If the entire optical path can be cryogenically cooled, the field of view is no longer limited by thermal baffling considerations and the thermal background from the telescope is significantly reduced. The only warm surfaces seen by the detector are the transparent window and a thin annulus around the pupil stop not masked by the nearest cold baffle. In our design this pupil stop is configured as a narcissus mirror with low emissivity and the detector sees only its own reflection. The area of this warm annulus is far less than the area of warm mirrors seen in conventional designs.

The remaining source of thermal background is the radiation from the window. Based on the absorption of IR grade SiO₂ at 2.4 μ m, we estimate that the combined emissivity of the two corrector elements is 0.25% in the K_{dark} passband. Furthermore, the lower ambient temperature in the Antarctic significantly reduces this source of background.

To reduce radiative heat loss from the window to the interior of the dewar, the cryogenically cooled baffles along the telescope tube (see Fig.6) will be machined to an ellipsoid shape and polished to reflect long wave emission back to the window. To avoid redirecting sky photons to the detector, a dichroic coating will be applied to the lower baffles to absorb in-band light and reflect longer wavelengths as was done for the VIRCAM baffles. The window radiates heat into a solid angle of π^2 steradians equally towards the interior volume. A non-sequential ray trace of the radiation shows that 73% of the radiation emitted by the window will exit back out the window. The remaining 27% of the radiation emitted by the window is absorbed/scattered by blackened surfaces on the central obstruction, back face of the baffles, or side wall between the baffles. The resulting residual radiative heat load from the window causes acceptable temperature depression and limits cooling requirements. Condensation on the window is prevented by desiccating air between the two menisci. Cooling of the outer surface is then less than the anticipated dew point. This baffling configuration was successfully used to reduce the radiative cooling of the MOSFIRE dewar window at Keck Observatory.

3.2 Manufacturing

All optical elements are being manufactured by Nu-Tek Precision Optical Corporation located in Aberdeen Maryland. The refractive lens elements have been polished and figured to their respective specifications and are awaiting deposition of the Anti-Reflection (AR) coating (see Fig.2). The primary mirror is a custom lightweight aluminum mirror designed by Nu-Tek (see Fig.3). Aluminum was chosen as the substrate material because of cost constraints. The primary mirror is fabricated from RSA-6061, which is needed to meet the surface figure and roughness specification of < 60 nm and < 2.5 nm rms respectively. RSA-6061 is a Rapidly Solidified Aluminum (RSA) material with very fine and homogeneous micro-structure. ¹⁰ With standard 6061 the surface roughness alone is estimated to be 10 to 20 nm rms from Single Point Diamond Turned (SPDT) polishing. This gives an estimated 2% Total Integrated Scatter (TIS) at $\lambda = 2 \mu m$ compared to 0.02% TIS for a surface that satisfies the < 2.5 nm specification. By using RSA-6061 bare aluminum material, it avoids needing a thin $\sim 150~\mu m$ thick nickel overcoat layer typically used on standard aluminum optics to achieve smooth surface finishes when operated at ambient temperature. Even a thin layer of nickel can be detrimental to optics in a cryogenic environment where the wavefront quality of the mirror can degrade because of a bi-metallic effect between the aluminum substrate and nickel overcoat.¹¹ The mirror structure is a single pocketed lightweight design connected to a supporting dome structure via a ring of flexures on the backside of the mirror (Fig.3). The flexures minimize the deflections on the mirror surface from gravity loads as the telescope is pointed to different elevation angles during observing. The domed supporting structure also has three circular cutouts that reduce its stiffness in key locations that have shown through Finite Element Analysis (FEA) to keep the surface deformation < 60 nm rms over any pointing of the telescope. The primary mirror is currently being figured to the desired specifications and estimated to be delivered this month.

3.3 Towards On-Sky Verification

Upon delivery, anticipated in August 2022, the optical elements will be tested as a system with a Zygo interferometer to measure the wavefront quality in air at room temperature, to confirm that they deliver the excellent wavefront quality predicted by the design and the manufacturer's surface metrology. Since all optical power is carried by the primary mirror there is negligible difference in the expected wavefront error (~ 20 nm) between the warm and cold prescriptions, provided that focus is preserved when cooled. To ensure this, the position of the primary will be offset with respect to the detector by $\sim 100~\mu m$ to account for both the change in radius of the mirror and thermal contraction of the relevant structural components.

After the objective is confirmed to deliver the desired wavefront quality in lab ambient conditions, it will be integrated into the cryostat and cooled to test thermal background and window temperature. For this test a highly polished metal cover will be placed over the first element, which is shaped to machining tolerances so that the detector sees only its own reflection. The temperatures of this narcissus mirror and the telescope enclosure will be adjusted independently to show that the thermal background scales as expected given the expected emissivity of the cover, and that background is not dominated by the black body radiation from the telescope.

The full opto-mechanical system will be tested on sky at Palomar Observatory where thermal background will be compared the Palomar's Widefield InfraRed Camera (WIRC) which is a conventional cryogenic re-imager with a cold stop. The 1.9" FWHM diffraction limited PSF of Cryoscope combined with the 1" median seeing in K-band on Palomar results in 2.1" estimated measured PSF FWHM on the detector array. This is 0.3 pixels wide where the PSF of the telescope is highly under-sampled. To confirm the on-sky diffraction limited image quality, a "virtual knife edge" test¹² will be done by taking the derivative of the signal as stars move across a pixel boundary then subtracting in quadrature the contribution from lateral charge diffusion typically measured. ¹³

4. THE VISION

Our ultimate goal is to build a wide-field IR surveyor in the Antarctic that is uniquely powerful for multimessenger astrophysics. To be sensitive to neutron star black hole mergers at 400 Mpc corresponding to the reach of LIGO-Virgo's fifth observing run in 2025, we aim to build a K-band surveyor that has a sensitivity of 23 mag while mapping 100 deg² per hour. This is comparable to the volumetric survey speed of LSST in y-band.¹⁴

To meet these science goals, we require survey speed that is unprecedented in the infrared. One can achieve this with a 1-m class cryogenic telescope with $50~\rm deg^2$ FoV located at the French-Italian base at Antarctic Dome C where the sky background is $40\times$ lower than temperate latitudes. At Dome C, the sky background in a \sim 225 nm wide passband centered on 2380 nm is expected to be even less than the $120~\mu \rm Jy/arcsec^2$ measured at the South Pole⁸ due to the higher elevation and lower temperatures. Furthermore, by mounting the telescope on a tower to place it above the 20 to 25 m thick boundary layer at Dome C, the median seeing will be a 0.25'' FWHM, 15 which is less than the 0.5'' FWHM for a diffraction limited PSF on a 1-m aperture f/2 telescope.

The uniform and high Strehl ratio over the field of view of the Cryoscope telescope design would deliver the highest possible sensitivity, while the fully cryogenic light path is expected to reduce thermal emission of the telescope to negligible levels, even compared to the K_{dark} sky. With exposure times adjusted to reach equivalent depth, we estimate that a 1-m cryogenic telescope would deliver a survey speed $140\times$ greater than the 4 m VISTA telescope due to the combination of wider field, darker sky and better seeing. Not included in this estimate are the additional gains from lower mirror temperature, higher transmission and the absence of warm support structures in the optical beam.

REFERENCES

- [1] Maksutov, D. D., "New catadioptric meniscus systems," Journal of the Optical Society of America (1917-1983) 34, 270 (May 1944).
- [2] Baker, J. G., "Correcting optical system," (U.S. Patent 3,022,708; Feb. 1962).
- [3] Houghton, J. L., "Lens system," (U.S. Patent 2,350,112; May 1944).

- [4] Wilson, J. C., Eikenberry, S. S., Henderson, C. P., Hayward, T. L., Carson, J. C., Pirger, B., Barry, D. J., Brandl, B. R., Houck, J. R., Fitzgerald, G. J., and Stolberg, T. M., "A Wide-Field Infrared Camera for the Palomar 200-inch Telescope," in [Instrument Design and Performance for Optical/Infrared Ground-based Telescopes], SPIE Conference Series 4841, 451–458 (Mar. 2003).
- [5] De, K., Hankins, M. J., Kasliwal, M. M., Moore, A. M., Ofek, E. O., Adams, S. M., Ashley, M. C. B., Babul, A.-N., Bagdasaryan, A., Burdge, K. B., Burnham, J., Dekany, R. G., Declacroix, A., Galla, A., Greffe, T., Hale, D., Jencson, J. E., Lau, R. M., Mahabal, A., McKenna, D., Sharma, M., Shopbell, P. L., Smith, R. M., Soon, J., Sokoloski, J., Soria, R., and Travouillon, T., "Palomar gattini-IR: Survey overview, data processing system, on-sky performance and first results," PASP 132, 025001 (Jan. 2020).
- [6] Sutherland, W., Emerson, J., Dalton, G., Atad-Ettedgui, E., Beard, S., Bennett, R., Bezawada, N., Born, A., Caldwell, M., Clark, P., Craig, S., Henry, D., Jeffers, P., Little, B., McPherson, A., Murray, J., Stewart, M., Stobie, B., Terrett, D., Ward, K., Whalley, M., and Woodhouse, G., "The Visible and Infrared Survey Telescope for Astronomy (VISTA): Design, technical overview, and performance," 575 (Mar. 2015).
- [7] Edgar, M. L., Zhelem, R., Waller, L., Kos, J., Mayfield, D., Pai, N., Sheinis, A., De Silva, G., Simpson, J., and Stazak, N., "Radioactive emission from high-index, optical glasses and atypical effects on CCDs," in [Advances in Optical and Mechanical Technologies for Telescopes and Instrumentation III], SPIE Conference Series 10706 (July 2018).
- [8] Li, Y., Zheng, J., Tuthill, P., Freeman, M., Ashley, M., Burton, M., Lawrence, J., Mould, J., and Wang, L., "Optimising the K Dark Filter for the Kunlun Infrared Sky Survey," 33 (Mar. 2016).
- [9] McLean, I. S., Steidel, C. C., Epps, H., Matthews, K., Adkins, S., Konidaris, N., Weber, B., Aliado, T., Brims, G., Canfield, J., Cromer, J., Fucik, J., Kulas, K., Mace, G., Magnone, K., Rodriguez, H., Wang, E., and Weiss, J., "Design and development of MOSFIRE: the multi-object spectrometer for infrared exploration at the Keck Observatory," in [Ground-based and Airborne Instrumentation for Astronomy III], SPIE Conference Series 7735 (July 2010).
- [10] Newswander, T., Crowther, B., Gubbels, G., and Senden, R., "Aluminum alloy AA-6061 and RSA-6061 heat treatment for large mirror applications," in [Material Technologies and Applications to Optics, Structures, Components, and Sub-Systems], SPIE Conference Series 8837 (Sept. 2013).
- [11] Folkman, S. L. and Stevens, M., "Characterization of electroless nickel plating on aluminum mirrors," in [Optomechanical Design and Engineering], SPIE Conference Series 4771, 254–264 (Sept. 2002).
- [12] Takacs, P. Z., Kotov, I., Frank, J., O'Connor, P., Radeka, V., and Lawrence, D. M., "PSF and MTF measurement methods for thick CCD sensor characterization," in [High Energy, Optical, and Infrared Detectors for Astronomy IV], SPIE Conference Series 7742 (July 2010).
- [13] Barron, N., Borysow, M., Beyerlein, K., Brown, M., Lorenzon, W., Schubnell, M., Tarlé, G., Tomasch, A., and Weaverdyck, C., "Subpixel response measurement of near-infrared detectors," PASP 119, 466–475 (Apr. 2007).
- [14] LSST Science Collaboration, "Lsst science book, version 2.0," (2009).
- [15] Lawrence, J. S., Ashley, M. C. B., Tokovinin, A., and Travouillon, T., "Exceptional astronomical seeing conditions above Dome C in Antarctica," 431, 278–281 (Sept. 2004).

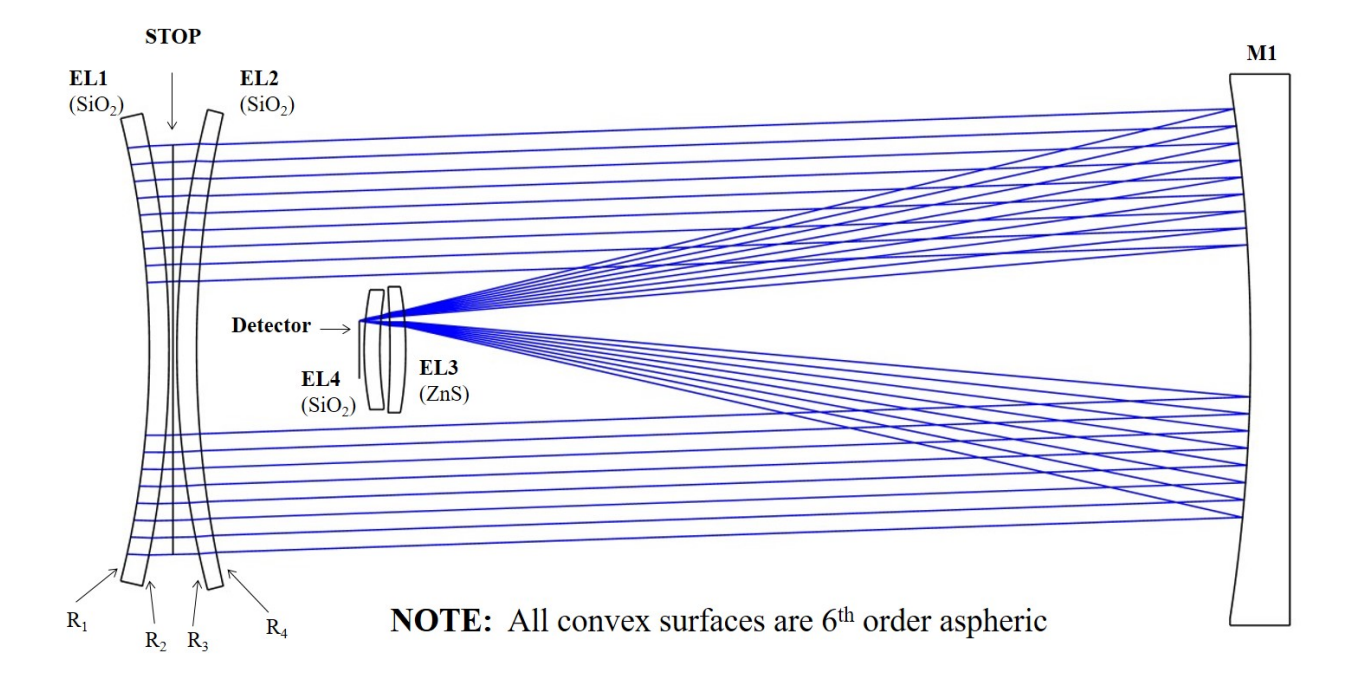


Figure 1: Optical layout for the Cryoscope telescope. Rays for the $+2^{\circ}$ field radius are shown in blue. The aperture stop and primary mirror are 26 and 35 cm in diameter respectively. The convex faces are all 6th order aspheric surfaces. The concave faces are all spherical surfaces.

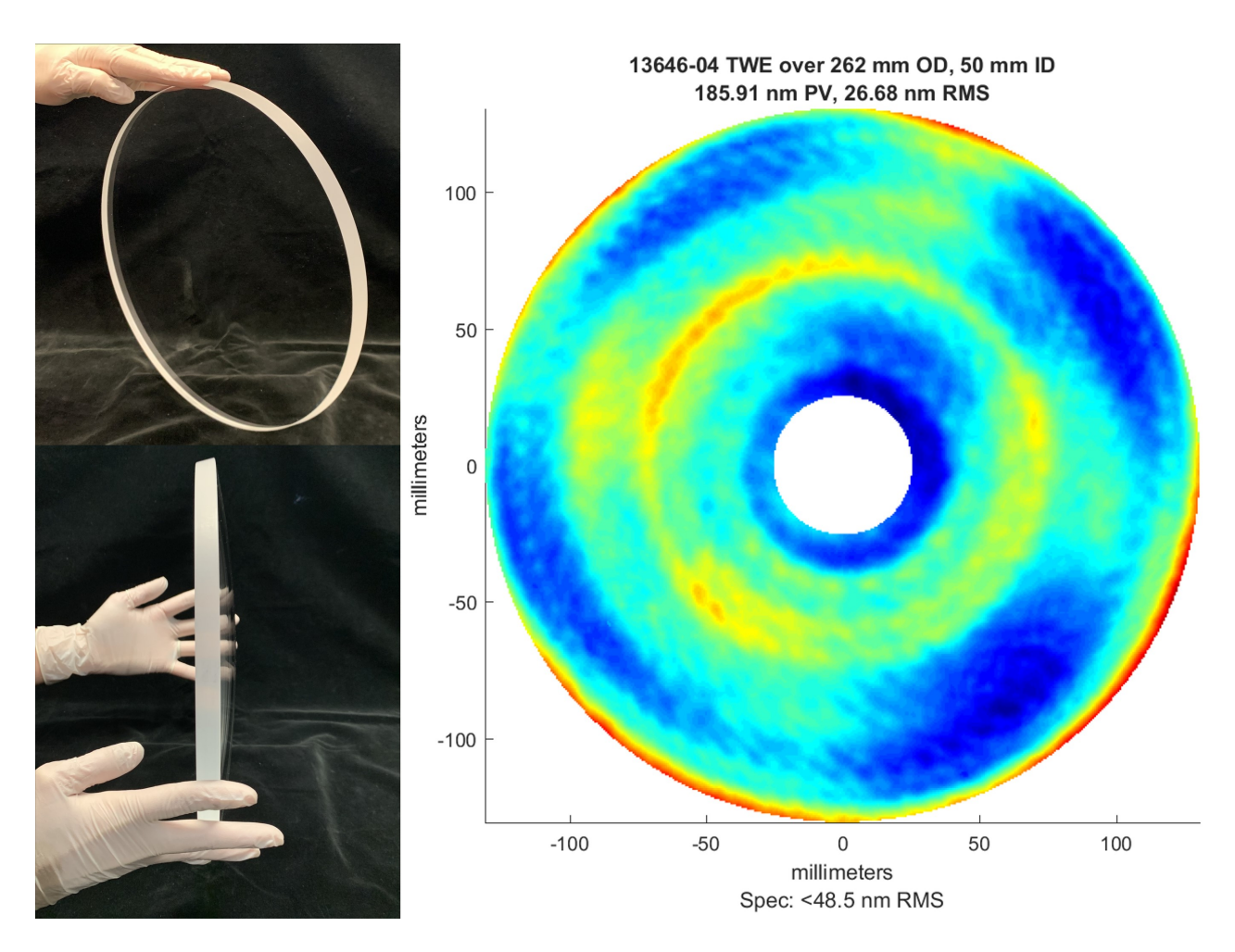


Figure 2: (*Left Panel*) Photos of the first meniscus corrector (EL1) prior to deposition of the AR coating manufactured by Nu-Tek. (*Right Panel*) Measured Transmitted Wavefront Error (TWE) by Nu-Tek with an error of 27 nm rms over the 262 mm clear aperture that exceeds the specification for < 48 nm rms. The central 50 mm diameter is excluded as this represents the area shadowed by the central obstruction.

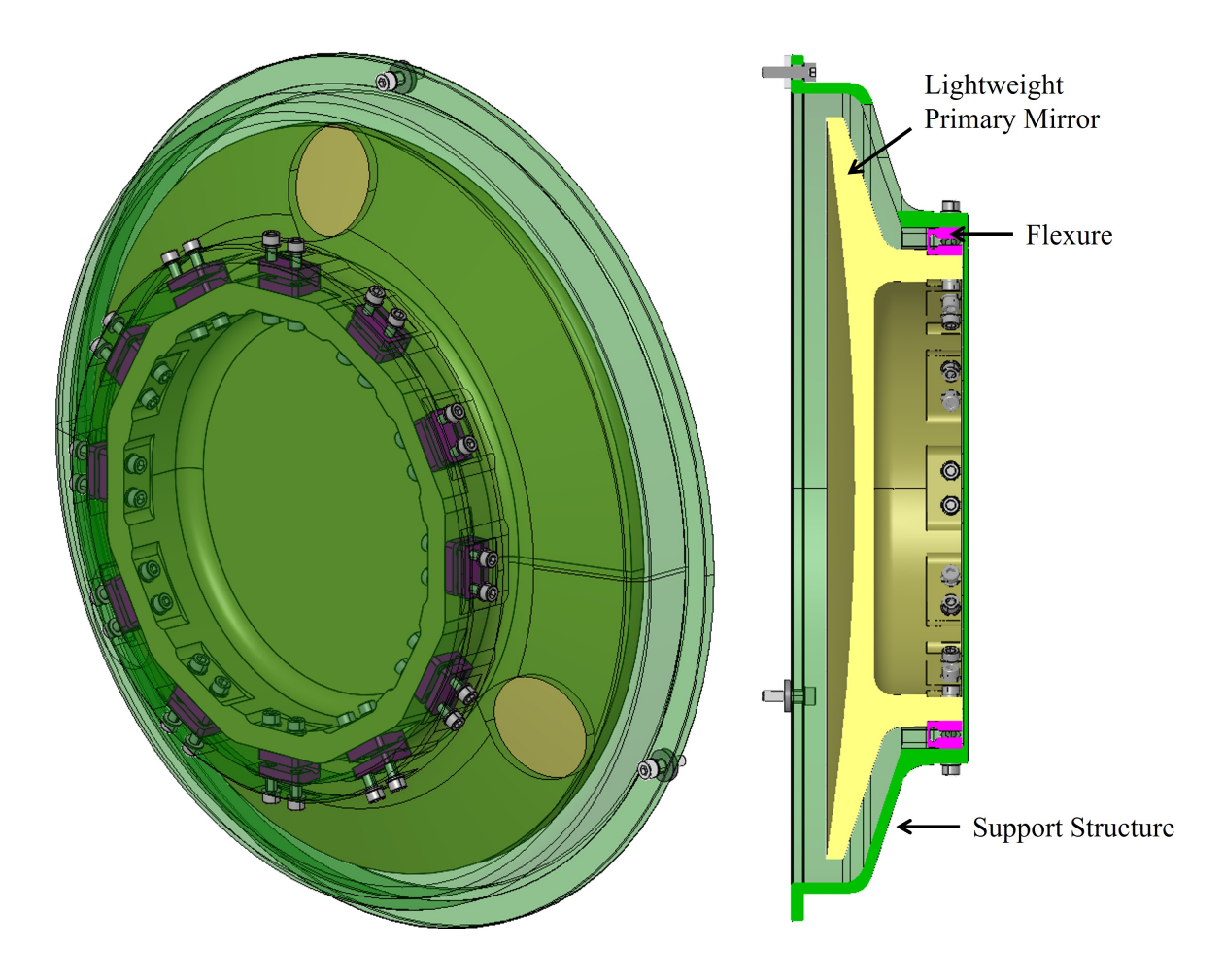


Figure 3: The Cryoscope lightweight bare aluminum primary mirror assembly designed by Nu-Tek. The assembly consists of the primary mirror (yellow) supported by a ring of flextures (pink) connect through a main support structure (green) that interfaces with internal radiation shield structure of the cryostat.

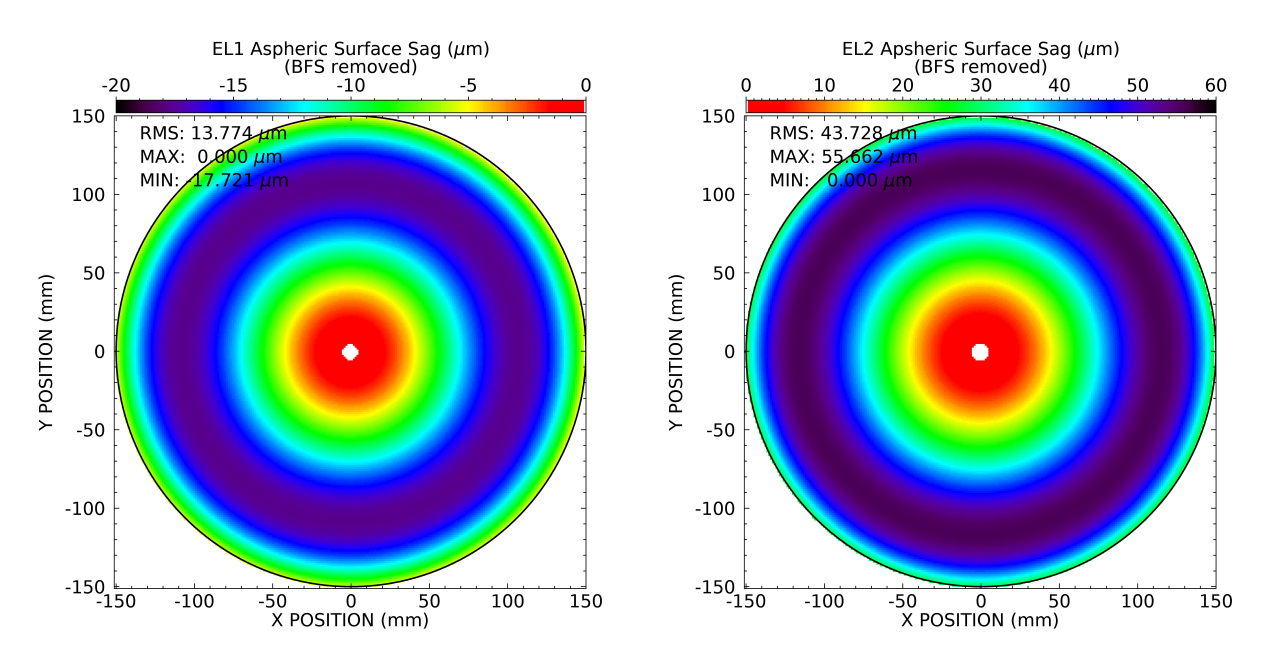


Figure 4: Aspheric surface sagitta (sag) of the meniscus corrector elements with the Best Fit Sphere (BFS) removed. The first and second corrector elements have a maximum deviation from a spherical surface of 18 μ m and 56 μ m with an rms of 14 μ m and 44 μ m across the surface respectively.

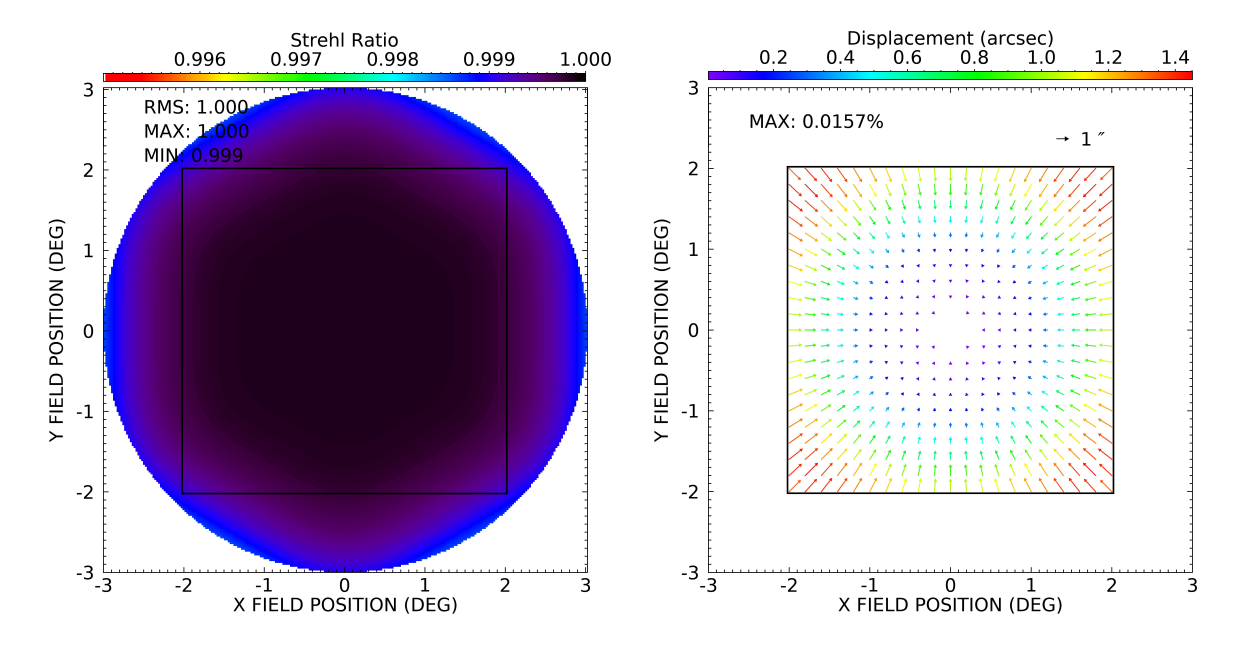


Figure 5: (Left Panel) A field map of the Strehl ratio for the polychromatic PSF from 1.99 to 2.55 μ m. The black box is the projected area of the detector on-sky. The telescope design delivers a nearly uniform \sim 99% Strehl ratio over the entire $4^{\circ} \times 4^{\circ}$ FoV. (Right Panel) A field map of the distortion. The arrows indicate the displacement from a regular grid in units of arc-seconds on-sky. The distortion pattern takes a pincushion form. There is a maximum distortion of 0.016% at the corners of the field.

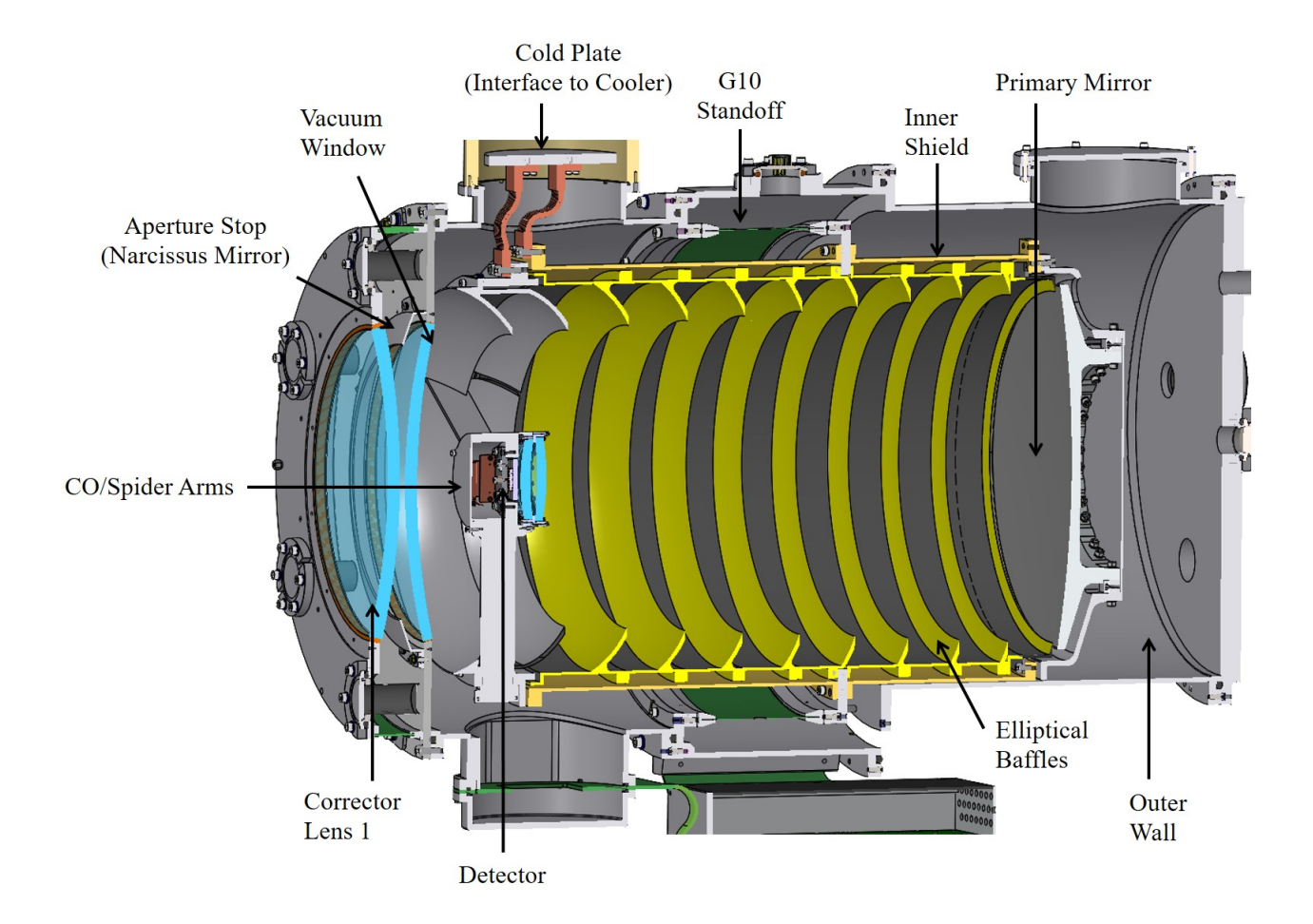


Figure 6: Mechanical layout for the Cryoscope dewar. The yellow baffles and two forward most baffles (near the central obstruction) have ellipsoidal surface profiles that both minimize stray light reaching the detector and self-heat the vacuum window to prevent condensation.